Local electron mean energy profile of positive primary streamer discharge with pin-plate electrodes in oxygen–nitrogen mixtures*

Sima Wen-Xia(司马文霞)†, Peng Qing-Jun(彭庆军), Yang Qing(杨 庆), Yuan Tao(袁 涛), and Shi Jian(施 健)

State Key Laboratory of Power Transmission Equipment & System Security and New Technology, Chongqing University, Chongqing 400044, *China*

(Received 18 May 2012; revised manuscript received 13 July 2012)

Local electron mean energy (LEME) has a direct effect on the rates of collisional ionization of molecules and atoms by electrons. Electron-impact ionization plays an important role and is the main process for the production of charged particles in a primary streamer discharge. Detailed research on the LEME profile in a primary streamer discharge is extremely important for a comprehensive understanding of the local physical mechanism of a streamer. In this study, the LEME profile of the primary streamer discharge in oxygen–nitrogen mixtures with a pin-plate gap of 0.5 cm under an impulse voltage is investigated using a fluid model. The fluid model includes the electron mean energy density equation, as well as continuity equations for electrons and ions and Poisson's electric field equation. The study finds that, except in the initial stage of the primary streamer, the LEME in the primary streamer tip tends to increase as the oxygen–nitrogen mole ratio increases and the pressure decreases. When the primary streamer bridges the gap, the LEME in the primary streamer channel is smaller than the first ionization energies of oxygen and nitrogen. The LEME in the primary streamer channel then decreases as the oxygen–nitrogen mole ratio increases and the pressure increases. The LEME in the primary streamer tip is primarily dependent on the reduced electric field with mole ratios of oxygen–nitrogen given in the oxygen–nitrogen mixtures.

Keywords: local electron mean energy profile, primary streamer discharge, electric field distribution, gas discharge

PACS: 52.65.–y, 52.25.Jm, 52.80.Hc, 52.25.Fi **DOI:** 10.1088/1674-1056/22/1/015203

1. Introduction

Low-temperature, non-equilibrium plasmas produced by gas discharges in air have recently received considerable attention because of their capability to enhance the reactivity of gas flows for various applications[1–9] in ozone production, pollution control, disinfection, surface treatment, ignition, and so on. Low-temperature, non-equilibrium plasmas from gas discharges usually take the form of streamer trees characterized by high electron and ion densities in a narrow channel.[10]

The concept of streamer discharge was introduced in the 1930s to explain naturally occurring spark discharges.[11] Streamer discharges are also regarded as the initial phase of spark discharges or the breakdown process of a gas, liquid, or solid. The characteristic duration of streamer propagation is relatively short. The streamer discharge is a nonlinear dynamics process of multi-field and multi-scale couplings.[12,13] The temporal scales include the electron transport time, the age of the excited particles, and the characteristic times for the formation and propagation of a streamer. The spatial scales include the collisional mean-free-path of electrons, the radius of the streamer channel, and the growth of interacting filamentary streamers comprising thousands of streamer branches.[10]

Great progress has been made in streamer discharge research during the last ten years. For example, the research group of multi-scale-modelling and nonlinear-dynamics (MAC3) led by Ebert has produced many significant works that have enhanced and developed streamer research.[10] Although the streamer discharge in gases is a random process from the physical viewpoint, according to research purposes, the random process of a streamer is usually ignored. Due to the missing out of the random process, three-dimensional (3D) simulations do not bring new results with respect to two-dimensional (2D) models. In fact, because 3D simulations of streamer discharge remain computationally expensive, there are still few 3D simulations. With the deepening of the study of streamer discharge, a full 3D simulation with the random process taken into account may be one of the main methods to investigate streamer discharge, which will provide a comprehensive understanding of it. The present study is mainly aimed at the local electron mean energy (LEME) profile of positive primary streamer discharge, so the simplified 2D axisymmetric model is a reasonable, acceptable, and a time-saving option. Various models have recently been developed to study streamer discharge. The main models include the kinetic model (e.g., PIC/MCC),[9,14–17] the fluid model[18,19] (through calculations using the moments of the Bolzmann equation),[20,21] and the hybrid kinetic–fluid model.[22–28] Each model has its own advantages and disadvantages. The kinetic models provide the most detailed kinetic information on elec-

*Project supported by the Funds for Innovative Research Groups of China (Grant No. 51021005), the National Basic Research Program of China (Grant No. 2009CB724504), and the National Natural Science Foundation of China (Grant No. 50707036).

†Corresponding author. E-mail: cqsmwx@cqu.edu.cn

© 2013 Chinese Physical Society and IOP Publishing Ltd

trons, ions, and atoms in the conventional low-pressure plasma discharges, but are very time-consuming.[23] The fluid models are widely used to investigate low-temperature plasmas from gas discharges.[21,29,30] The hybrid model combines the advantages of the kinetic and the fluid models. Recently, Li *et al.* from MAC3 have made some progress in the application of a hybrid kinetic–fluid model for streamer discharge analysis.[22–26] The hybrid kinetic–fluid model could be one of the main models used in future streamer discharge studies, but the fluid model is currently used for investigations. The research on streamer discharges continues to focus on the anode current, streamer propagation velocity, channel diameter, electric field, and photoionization. However, the local electron mean energy density equation is usually ignored in most studies.[18,19]

In low-temperature, non-equilibrium plasma discharges, the LEME is very important for understanding the local mechanisms of streamer discharge. For example, the propagation velocities of ion-acoustic waves, the electronic mean free path in plasma, the electron diffusion coefficients, conductivity, and thermal conductivity are calculated based on the LEME or the electron temperature equaling the LEME multiplied by 2/3.[31] Moreover, electrons cause the energy transfer in streamer discharge. The collision ionization by electrons is the main process for the production of charged particles in low-temperature, non-equilibrium plasmas from gas discharges. The rate coefficients for electron impact ionization, as well as the electron diffusion coefficient and mobility, are generally functions of the LEME.[20] Although the LEME is important in the analysis of low-temperature, non-equilibrium plasmas from gas discharges, the current understanding of the LEME in streamer discharges remains incomplete. The streamer discharge usually includes a primary steamer and a secondary streamer. This study aims to examine the LEME profile of the positive primary streamer discharge with pin-plate electrodes in an oxygen–nitrogen mixture. This paper is arranged as follows. Section 2 presents a brief description of the model. Section 3 presents the results and discussion. Section 4 presents the summary and conclusion.

2. Mathematical model

2.1. Governing equations

The electron conservation and the LEME density equations are given by[20,21,30]

$$\frac{\partial n_{\rm e}}{\partial t} + \nabla \cdot \boldsymbol{\Gamma}_{\rm e} = R_{\rm e}, \tag{1}$$

$$\boldsymbol{\Gamma}_{\rm e} = -\mu_{\rm e} \boldsymbol{E} n_{\rm e} - \nabla (D_{\rm e} n_{\rm e}); \tag{2}$$

$$\frac{\partial}{\partial t}(n_{\rm e}\bar{\varepsilon}) + \nabla \cdot \boldsymbol{\Gamma}_{\varepsilon} = -e\boldsymbol{\Gamma}_{\rm e} \cdot \nabla\varphi + e\sum_{i=1}^{I_g} \Delta\varepsilon_i^{\rm e} R_i, \tag{3}$$

$$\boldsymbol{\Gamma}_{\varepsilon} = n_{\rm e}\bar{\varepsilon}\mu_{\varepsilon}\nabla\varphi - D_{\varepsilon}\nabla n_{\rm e}\bar{\varepsilon}, \tag{4}$$

where $n_{\rm e}$ is the electron density; $\boldsymbol{\Gamma}_{\rm e}$ is the electron density flux; $R_{\rm e}$ is the electron production/destruction rate attributed to ionization or recombination, the photoionization processes, and the secondary emission processes on the cathode; $\mu_{\rm e}$ and $D_{\rm e}$ are the electron mobility and diffusion coefficients, respectively; $\bar{\varepsilon}$ is the LEME; $\boldsymbol{\Gamma}_{\varepsilon}$ is the electron energy flux; e is the unit charge; $\Delta\varepsilon_i^{\rm e}$ is the energy lost per electron in an inelastic collision described by gas reaction i; R_i is the rate of progress of reaction i with electron participation; μ_{ε} and D_{ε} are the electron energy mobility and diffusion coefficients, respectively; and φ is the electrostatic potential. The aforementioned transport coefficients of electrons are obtained by solving the Boltzmann equation.[20,32]

The governing equations for ions and neutral particles are given by[18]

$$\frac{\partial n_k^+}{\partial t} = R_{\rm ion} + R_{\rm photo} - R_{\rm rec}^{\rm ei} - R_{\rm rec}^{\rm ii}, \tag{5}$$

$$\frac{\partial n_k^-}{\partial t} = R_{\rm att} - R_{\rm rec}^{\rm ii}, \tag{6}$$

$$\frac{\partial n_{\rm n}}{\partial t} = R_{\rm rec}^{\rm ei} + R_{\rm rec}^{\rm ii} - R_{\rm ion} - R_{\rm photo} - R_{\rm att}, \tag{7}$$

where n_k^+, n_k^-, and $n_{\rm n}$ represent positive ions, negative ions, and neutral particles, respectively; $R_{\rm ion}$, $R_{\rm photo}$, $R_{\rm rec}^{\rm ei}$, $R_{\rm rec}^{\rm ii}$, and $R_{\rm att}$ are the rates of ionization, photoionization, electron–ion, ion–ion recombination, and electron attachment, respectively. The $R_{\rm photo}$ is given by[18,33]

$$R_{\rm photo} = \frac{1}{4\pi}\frac{p_q}{p+p_q}\int {\rm d}^3 r_1 \frac{R_{\rm ion}}{|\boldsymbol{r}-\boldsymbol{r}_1|^2} h(|\boldsymbol{r}-\boldsymbol{r}_1|\,p), \tag{8}$$

where $\boldsymbol{r}$ is the observation point, $\boldsymbol{r}_1$ is the source point, p_q is the quenching pressure of the singlet state of N_2, p is the gas pressure, and $h(|\boldsymbol{r}-\boldsymbol{r}_1|\,p)$ is the absorption function of the photoionizing radiation. The Eddington approximation method is used to calculate $R_{\rm photo}$.[34]

According to the local field approximation of the electric field, the electric field in the discharge gap is calculated using Poisson's equation[18,35]

$$\varepsilon\nabla^2\varphi = -e\left(\sum_k n_k^+ - \sum_k n_k^- - n_{\rm e}\right), \tag{9}$$

where ε is approximately the permittivity of air.

2.2. Boundary conditions

Figure 1(a) shows a schematic diagram of the primary streamer discharge device. The discharge of an oxygen–nitrogen mixture at an atmospheric pressure is sustained by an impulse voltage. Only half of the geometry is simulated because of the symmetry. Figure 1(b) shows the computational domain for the primary streamer discharge of a positive pin-plane gap. Line a–b is the symmetry axis. The boundary a–f–e represents the anode. The boundary b–c is the grounded

substrate. Zero-charge boundary conditions $[\boldsymbol{n}\cdot(\varepsilon\nabla\varphi)=0]$ are used at boundary *c*–*d*–*e*.[28] The electron flux at the electrode is expressed as[36]

$$\boldsymbol{\Gamma}_{\mathrm{e}}\cdot\boldsymbol{n}=\frac{1-\gamma_{\mathrm{e}}}{1+\gamma_{\mathrm{e}}}\left[-(2a_{\mathrm{e}}-1)\,\mu_{\mathrm{e}}\boldsymbol{E}\cdot\boldsymbol{n}n_{\mathrm{e}}+\frac{1}{2}v_{\mathrm{e,th}}n_{\mathrm{e}}\right], \quad (10)$$

where $\boldsymbol{n}$ is the boundary normal vector, γ_{e} is the fraction of electrons reflected by the surface of electrode (sometimes called the classical secondary emission coefficient), and $v_{\mathrm{e,th}}=\sqrt{8k_{\mathrm{B}}T_{\mathrm{e}}/\pi m_{\mathrm{e}}}$ is the electron thermal velocity.[28] The a_{e} is equal to 1 when the electron flux is directed toward the electrode and zero otherwise. The electron energy density flux $\boldsymbol{\Gamma}_{\varepsilon}$ to the electrodes (boundaries *a*–*f*–*e* and *b*–*c*) is[37]

$$\boldsymbol{\Gamma}_{\varepsilon}\cdot\boldsymbol{n}=\frac{1}{3}v_{\mathrm{e,th}}\bar{\varepsilon}n_{\mathrm{e}}. \quad (11)$$

Because of reactions at the electrode surface, the ions and unstable neutral particles are quenched and transformed into stable neutral particles, which then return to the pin-plate gap (For example, $N_2^+\rightarrow N_2$, $O_2^+\rightarrow O_2$, $O_2^-\rightarrow O_2$, $O\rightarrow O_2$). The ion fluxes at the electrode are expressed as[28]

$$\boldsymbol{\Gamma}_i\cdot\boldsymbol{n}=\frac{\gamma_i}{4}\sqrt{\frac{8k_{\mathrm{B}}T}{\pi m_i}}n_i, \quad (12)$$

where $\boldsymbol{\Gamma}_i$ and n_i are the flux density and the particle number of species *i*, respectively; γ_i is the surface interaction coefficient, which specifies the probability that species *i* will react at the surface; and m_i is the ion mass of species *i*. At boundary *c*–*d*–*e*, the normal gradients of all species densities are zero.

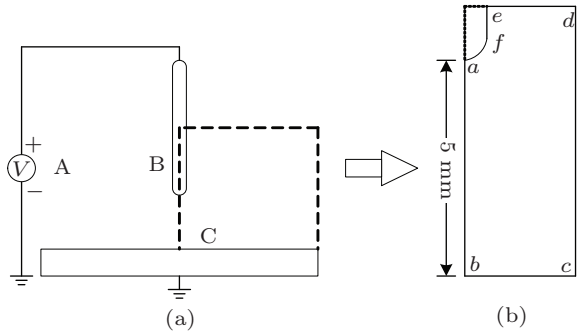


Fig. 1. Geometric model used in the simulation. (a) Schematic diagram of the pin-plate streamer discharge; (b) computational domain.

2.3. Numerical algorithm

The model used in this study has a two-dimensional axial symmetry configuration, as shown in Fig. 1(b). The model is implemented using a COMSOL Multiphysics® package based on the finite-element method. A fully implicit time-marching method is used for the transport equations and the Poisson equation. All numerical experiments are conducted using a computer with two 3.4 GHz Intel(R) I7-2600 processors in 64-bit mode running in parallel and 16 GB memory, all running on Windows 7. The primary streamer discharge occurs in the vicinity of the primary streamer tip and propagates along the axial direction. Therefore, a very fine unstructured mesh (Fig. 2) is used around the needle head and along the axial symmetry line. The mesh parameters are shown in Table 1. The quality of the elements of the mesh is an important consideration.[38] Based on Table 1, the minimum element quality and the average element quality are 0.8503 and 0.9846, respectively.

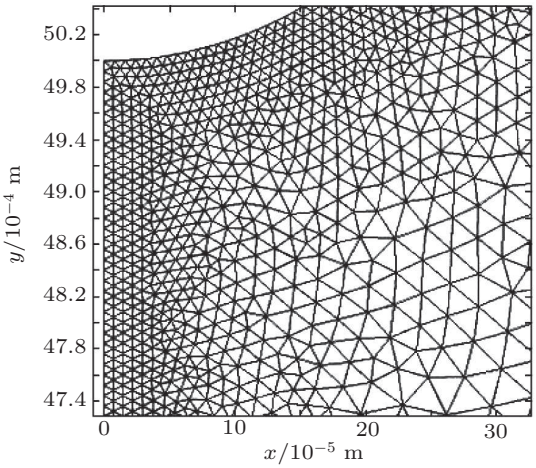


Fig. 2. Unstructured mesh used.

Table 1. Mesh statistics.

Mesh parameter	Value
Triangular elements	39,854
Edge elements	1,000
Minimum element quality	0.8503
Average element quality	0.9846
Element area ratio	0.01044
Mesh area/m^2	2.187×10^{-5}

2.4. Plasma chemistry

Chemical reaction schemes are important for streamer discharge simulations. Sentman *et al.*[39] and Gordillo–Vazquez[40] recently used complex chemical reaction schemes when the characteristic duration of the discharge reaches tens of microseconds or even tens of seconds. However, the characteristic duration of a primary streamer only lasts several nanoseconds. Based on the time scales of primary streamers and according to Pancheshnyi's research,[18] the degrees of excitation, dissociation, and ionization of oxygen–nitrogen mixture are relatively low, and the heating of the primary streamer channel is negligible. Therefore, the chemical reaction schemes reported in the current study include e, N_2^+, O_2^+, $O_2^+N_2$, N_4^+, O_4^+, O_2^-, O and O_3, as well as 18 reactions with their participation.

1) Electron impact ionization processes

$$\mathrm{R1}:\ \mathrm{e}+\mathrm{N_2}\rightarrow 2\mathrm{e}+\mathrm{N_2^+},\quad k_1(\varepsilon),\ \Delta\bar{\varepsilon}_1^{\mathrm{e}}=12.06\ \mathrm{eV}, \quad (13)$$

$$\mathrm{R2}:\ \mathrm{e}+\mathrm{O_2}\rightarrow 2\mathrm{e}+\mathrm{O_2^+},\quad k_2(\varepsilon),\ \Delta\bar{\varepsilon}_2^{\mathrm{e}}=15.6\ \mathrm{eV}. \quad (14)$$

The rate coefficients $k_1(\varepsilon)$ and $k_2(\varepsilon)$ are calculated from collision cross-section data using the Boltzmann equation.[20]

2) Charge-transfer processes

$$\mathrm{R3}: \mathrm{N_2^+ + N_2 + } M \rightarrow \mathrm{N_4^+} + M, \quad k_3 = 5\times10^{-41}\ \mathrm{m^6/s}, \quad (15)$$

$$\mathrm{R4}: \mathrm{N_2^+ + O_2 \rightarrow O_2^+ + N_2}, \quad k_4 = 6\times10^{-17}\ \mathrm{m^3/s}, \quad (16)$$

$$\mathrm{R5}: \mathrm{N_4^+ + O_2 \rightarrow O_2^+ + 2N_2}, \quad k_5 = 2.5\times10^{-16}\ \mathrm{m^3/s}, \quad (17)$$

$$\mathrm{R6}: \mathrm{2N_2 + O_2^+ \rightarrow O_2^+N_2 + N_2}, \quad k_6 = 9\times10^{-43}\ \mathrm{m^6/s}, \quad (18)$$

$$\mathrm{R7}: \mathrm{O_2^+N_2 + N_2 \rightarrow O_2^+ + 2N_2}, \quad k_7 = 4.3\times10^{-10}\ \mathrm{m^3/s}, \quad (19)$$

$$\mathrm{R8}: \mathrm{O_2^+N_2 + O_2 \rightarrow O_4^+ + N_2}, \quad k_8 = 1\times10^{-15}\ \mathrm{m^3/s}, \quad (20)$$

$$\mathrm{R9}: \mathrm{O_2^+ + O_2 +}M \rightarrow \mathrm{O_4^+} + M, \quad k_9 = 2.4\times10^{-42}\ \mathrm{m^6/s}. \quad (21)$$

3) Reaction of positive ions, negative ions, and neutral particles

$$\mathrm{R10}: \mathrm{O_4^+ + e \rightarrow 2O_2}, \quad k_{10} = 1.4\times10^{-12}(300/T_\mathrm{e})^{0.5}\ \mathrm{m^3/s}, \quad (22)$$

$$\mathrm{R11}: \mathrm{O_2^+ + e \rightarrow 2O}, \quad k_{11} = 2\times10^{-13}(300/T_\mathrm{e})\ \mathrm{m^3/s}, \quad (23)$$

$$\mathrm{R12}: \mathrm{O_4^+ + O_2^- \rightarrow 3O_2}, \quad k_{12} = 1\times10^{-13}\ \mathrm{m^3/s}, \quad (24)$$

$$\mathrm{R13}: \mathrm{O_4^+ + O_2^- +}M \rightarrow \mathrm{3O_2} + M, \quad k_{13} = 2\times10^{-37}\ \mathrm{m^6/s}, \quad (25)$$

$$\mathrm{R14}: \mathrm{O_2^+ + O_2^- +}M \rightarrow \mathrm{2O_2} + M, \quad k_{14} = 2\times10^{-37}\ \mathrm{m^6/s}, \quad (26)$$

$$\mathrm{R15}: \mathrm{O + O_2 +}M \rightarrow \mathrm{O_3} + M, \quad k_{15} = 2.5\times10^{-46}\ \mathrm{m^6/s}, \quad (27)$$

$$\mathrm{R16}: \mathrm{2e + N_2^+ \rightarrow e + N_2}, \quad k_{16} = 5.651\times10^{-27}T_\mathrm{e}^{-0.8}\ \mathrm{m^6/s}, \quad (28)$$

$$\mathrm{R17}: \mathrm{e + N_2^+ + N_2 \rightarrow 2N_2}, \quad k_{17} = 6.07\times10^{-34}T_\mathrm{e}^{-2.5}\ \mathrm{m^6/s}. \quad (29)$$

4) Electron attachment process

$$\mathrm{R18}: \mathrm{2O_2 + e \rightarrow O_2^- + O_2}, \quad k_{18} = 2\times10^{-41}(300/T_\mathrm{e})\ \mathrm{m^6/s}. \quad (30)$$

The rate coefficients k_3–k_{18} are found in the literature.[18,41–43] The electron temperature T_e is given by $T_\mathrm{e} = 2\bar{\varepsilon}/3$ and is presented in units of K.

3. Results and discussion

Based on Pancheshnyi's work,[18] the plasma cloud of the initial primary streamer exhibits a Gaussian distribution in the space close to the pin electrode

$$\sum_j n_j^-(r,z)\Big|_{t=0} + n_\mathrm{e}(r,z)|_{t=0} = \sum_i n_i^+(r,z)\Big|_{t=0} = n_0 \exp\left[-(r/\sigma_r)^2 - ((z-z_0)/\sigma_z)^2\right], \quad (31)$$

where $n_0 = 10^{14}\ \mathrm{cm^{-3}}$, $\sigma_z = 0.1$ mm, $\sigma_r = 0.05$ mm, $n_\mathrm{e}(r,z)$, $n_j^-(r,z)$, and $n_i^+(r,z)$ denote the electron, negative ion, and positive ion densities, respectively, and subscript i denotes $\mathrm{N_2^+}$, $\mathrm{O_2^+}$, $\mathrm{O_2^+N_2}$, $\mathrm{N_4^+}$, and $\mathrm{O_4^+}$. The electron density is significantly greater than the negative ion density at $t = 0$ ns, that is, $n_\mathrm{e} \gg \sum n_j^-$.

Ono *et al.*[3] reported observations of cathode-directed primary streamers in air-filled, point-plane gaps that are 0.5 cm in length. He found that the primary streamer reaches the cathode in 7 ns. For comparison, the current study uses the same conditions as those used by Ono. The atmospheric pressure is set at 300 K. An applied voltage $V(t)$ with an amplitude of 24 kV is used as the impulse voltage. The rise time of $V(t)$ is set to 0.05 μs, and with a 0.2 μs decay, which is half of the peak value. The radius of the positive pin electrode is set to 0.3 mm, and the pin-plate gap is set to 0.5 cm. To facilitate calculations, the air is simplified to an oxygen–nitrogen mixture with an oxygen to nitrogen ratio of 2:8.

3.1. Electric field distribution and streamer propagation velocity

A comparison between the electric field and the streamer velocity is performed to verify the validity of the model. The electrons in the primary streamer are accelerated by an electric field. The electrons move toward the pin anode, and some are consumed at the anode or in the primary streamer channel. The positive ions move toward the cathode, but their velocities are substantially lower than those of the electrons. As a result, the positive charge density becomes greater than the negative charge density in the primary streamer head, as shown in Fig. 3. According to the local approximation of the electric field,[31,35] the electric field of the primary streamer head is strengthened, as shown in Figs. 4 and 5. The electric field at the primary streamer head ranges from 1×10^7 V/m to 1.83×10^7 V/m. The electric field near the plane cathode ranges from 1.3×10^6 V/m to 3.9×10^6 V/m. In Ref. [19], the electric field at a primary streamer tip with a 0.1 cm gap was a constant of approximately 2×10^7 V/m, and the electric field near the cathode ranged from 1×10^6 V/m to 3×10^6 V/m.

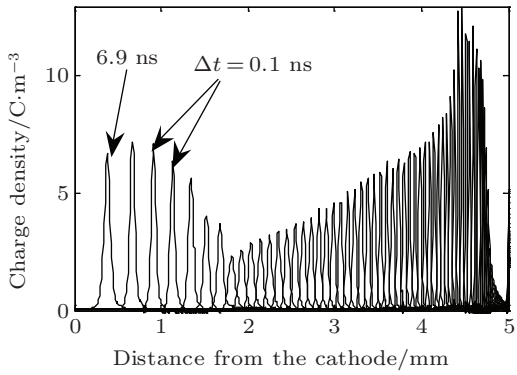


Fig. 3. Charge density distribution along the axis of symmetry.

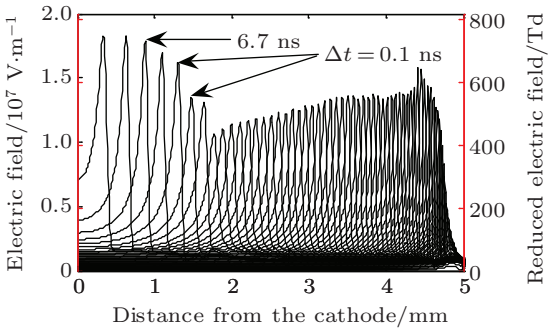


Fig. 4. Electric field distribution along the axis of symmetry.

Based on Ono's work[3] the average velocity of primary streamers is approximately 7.14×10^5 m/s in air-filled, point-plane gaps that are 0.5 cm in length. In the current study, the primary streamer bridges the whole gap in 6.9 ns, as shown in Fig. 5(c), and its average velocity is approximately 7.2×10^5 m/s under the same conditions as those in Ono's experiment.[3] The velocities of streamer propagations reported in the existing literature are approximately 10^6 m/s, but the results under similar conditions may differ by up to an order of magnitude.[44] Therefore, only general comparisons with numerical results of streamer propagation velocities are performed in the current study. Based on Luque's definition of streamer radius,[45] the primary streamer radii in the current study are shown in Fig. 6. The primary streamer mean radius reported in this paper is approximately 0.358 mm (with a diameter of 0.716 mm). The mean velocity of primary streamer propagation calculated with the completely empirical relation proposed by Briels *et al.*[46] is 2.56×10^5 m/s.

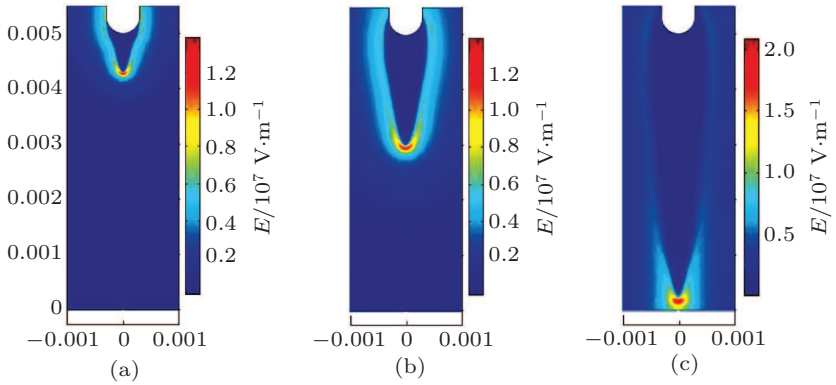


Fig. 5. (color online) Electric field distributions over an axial cross-section at (a) 3 ns, (b) 5 ns, and (c) 6.9 ns.

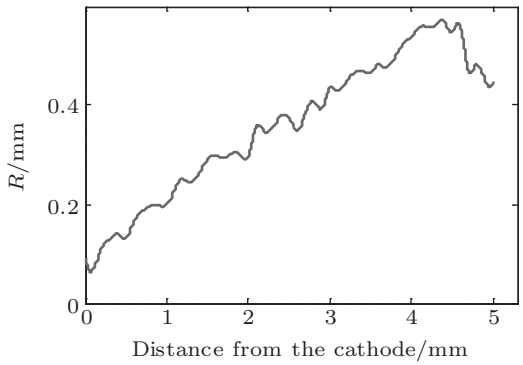


Fig. 6. Radii of the primary streamer channel.

Figure 7 shows the velocity of the primary streamer propagation calculated from the model using the discharge parameters in Fig. 3. The velocity of the primary streamer propagation increases over time t, reaching approximately 3.00×10^6 m/s at $t = 6.9$ ns. The aforementioned velocity–time (v–t) characteristic is similar to that observed by Sigmond.[47] Sigmond reported streak photographic observations of cathode-directed primary streamers in air-filled, point-plane gaps that are 0.5 cm and 1.0 cm in length. He found that primary streamer velocities increase as the distance from the cathode decreases, reaching approximately 1×10^6 cm/s at the plane cathode. The primary streamer velocity at the plane cathode reported in the current study is larger than that reported by Sigmond. Based on Winands' work,[48] the differences between the streamer velocity at the plane cathode in the current paper and that reported by Sigmond[47] may have been influenced by the applied electric field and/or the voltage rise rate.

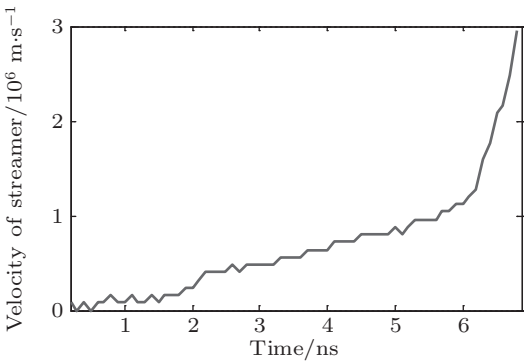


Fig. 7. Velocity of the primary streamer propagation.

The electric field distribution and the velocity of the primary streamer propagation obtained in the current study coincide with those of the other studies. Therefore, the model and the calculations used in the current study are valid.

3.2. Effect of oxygen and nitrogen mole ratio on the LEME profile

Figure 8 shows the calculated LEME and the reduced electric field in the primary streamer tip, which satisfy all the conditions in Subsection 3.1 except for the oxygen and nitrogen mole ratio. The effect of the oxygen and nitrogen mole ratio on the LEME profile is ignored when the z coordinate of the streamer tip ranges from 4.6 mm to 5 mm, as shown in Fig. 8(a). The LEME in the primary streamer tip increases as the oxygen and nitrogen mole ratio increases when the z coordinate of the streamer tip ranges from 0.42 mm to 4.6 mm. The reason for the aforementioned behavior is that the electron-energy loss in the impact ionization process increases as the oxygen and nitrogen mole ratio increases, because oxygen has a smaller first ionization energy compared with that of nitrogen. In Ref. [47], Sigmond estimated that the LEME in the streamer head ranges from 12 eV to 16 eV and the reduced electric field of the streamer head ranges from 400 Td to 600 Td in the air streamer discharge. Air is regarded as an oxygen–nitrogen mixture with an oxygen and nitrogen mole ratio of approximately 2:8. In the current study, the LEME in the streamer head ranges from 13.9 eV to 21.9 eV in the region where the z coordinate of streamer tip ranges from 0.42 mm to 4.6 mm with the reduced electric field ranging from 430 Td to 800 Td, as shown in Fig. 8. The LEME–reduced electric field ($\bar{\varepsilon}$–E/N) characteristic coincides with Sigmond's studies.

When the oxygen and nitrogen mole ratio is 3:7, the LEME in the primary streamer tip reaches 35 eV and has a reduced electric field of 1300 Td, as shown in Fig. 8(b). The resulting values are slightly large for a primary streamer discharge. The slightly large values are likely attained because the kinetic scheme of the primary streamer reported in this study does not include the excitation process of gas molecules. The electron-energy loss in the kinetic scheme is smaller than that in the actual discharge process. A smaller electron-energy loss results in a larger LEME in the primary streamer. Therefore, the LEME is an important factor to be considered when the complete kinetic scheme for oxygen–nitrogen mixtures is simplified to the reasonable kinetic scheme of a primary streamer. When the oxygen and nitrogen mole ratio is 1:9, the maximum value of the LEME in the primary streamer head is only 16.1 eV, with a reduced electric field of 500 Td, as shown in Fig. 8(b). In the region where the z coordinate of the streamer tip ranges from 1.8 mm to 4.6 mm, the difference between the LEMEs obtained with oxygen and nitrogen mole ratios of 2:8 and 1:9 is nearly a constant value of 2.8 eV. However, the difference between the reduced electric fields obtained from oxygen and nitrogen mole ratios of 2:8 and 1:9 increases as the distance from the cathode decreases, as shown in Fig. 8(b). In the region where the z coordinate of the streamer tip ranges from 0.42 mm to 1.8 mm, which is the region near the cathode surface, the LEME increases as the distance from the cathode decreases. The aforementioned behavior may be attributed to the effect of the cathode on the discharge, i.e., the electric field near the cathode surface is strengthened because of the space charge in the cathode surface.

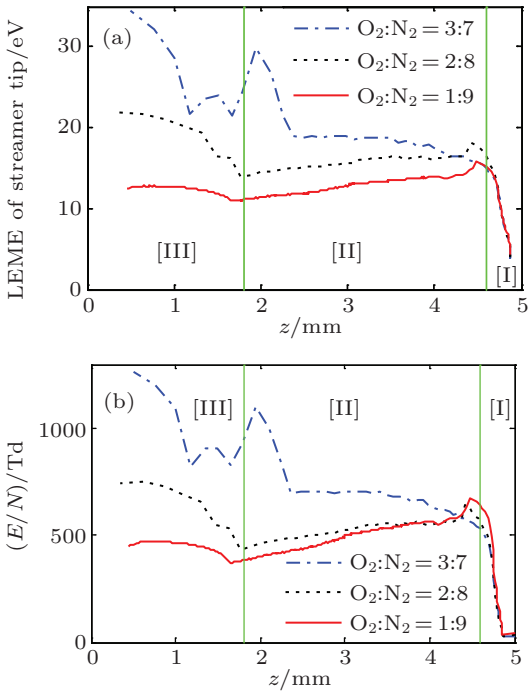


Fig. 8. (color online) (a) LEME and (b) reduced electric field in the primary streamer tip.

Figure 9 shows the LEME and the reduced electric field profiles along the axis of symmetry when the primary streamer bridges the gap. The LEME in the primary streamer channel ranges from 4.47 eV to 6 eV, and the reduced electric field ranges from 28.4 Td to 62 Td. The LEME in the primary streamer channel slightly increases as the oxygen and nitrogen mole ratio decreases. As reported in our previous paper,[29] although the proportion of N_2 (approximately 78%) is significantly higher than that of O_2 (approximately 22%) in air, in a streamer discharge, the main contributor to electron production is the ionization of O_2. Therefore, the electron density in the primary streamer channel increases as the oxygen and nitrogen mole ratio increases. In Eq. (3), the electron energy loss/gain attributed to inelastic collisions is given by

$$e\sum_{i=1}^{I_g}\Delta\varepsilon_i^e R_i = e\sum_{i=1}^{I_g}\Delta\varepsilon_i^e k_i n_e n_i, \tag{32}$$

where k_i and n_i are the reaction rate coefficient and the background gas density, respectively. Although the mean-electron-energy loss in the oxygen–nitrogen mixture decreases as the

oxygen and nitrogen mole ratio increases, the total energy transfer $e\sum\Delta\varepsilon_i^e k_i n_e n_i$ increases because the electron density significantly increases. Therefore, in the primary streamer channel, the total energy transfer increases as the oxygen and nitrogen mole ratio increases, and the LEME in the primary streamer channel decreases, as shown in Fig. 9(a). In the region of 2.3 mm to 5 mm away from the cathode, the variations in the LEMEs at different oxygen and nitrogen mole ratios are similar, with intervals of approximately 0.43 eV and 0.13 eV, respectively. However, Fig. 9(b) shows that the reduced electric field in the region of 2.3 mm to 5 mm away from the cathode, with an oxygen and nitrogen mole ratio of 1:9, is approximately equal to that with an oxygen and nitrogen mole ratio of 2:8 and is 7.32 Td smaller than that with an oxygen and nitrogen mole ratio of 3:7. Because of the effect of streamer tip charge, fluctuation in the LEME and a reduced electric field are observed in the region of 1.4 mm to 2.3 mm away from the cathode. Figures 8(a) and 9(a) show that the LEME in the primary streamer tip is larger than the first ionization energies of oxygen and nitrogen. Therefore, the impact ionizations of nitrogen and oxygen molecules mainly occur in the primary streamer head.

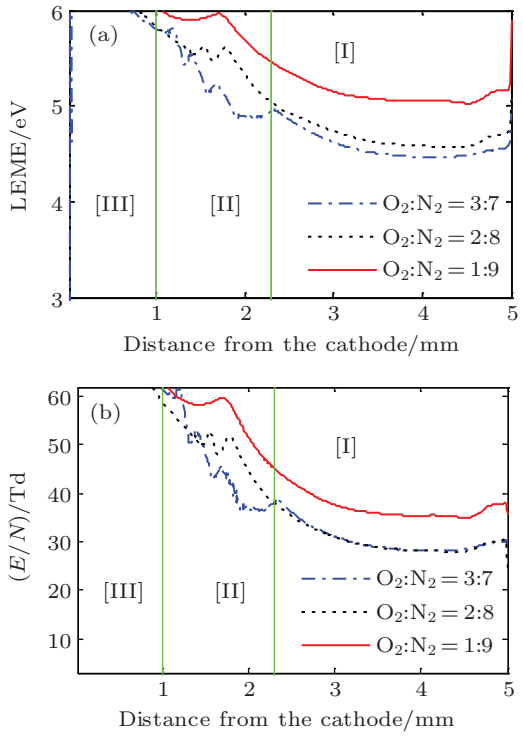


Fig. 9. (color online) (a) LEME and (b) reduced electric field profiles along the axis of symmetry for primary streamers bridging the gap.

3.3. Effect of pressure on the LEME profile

Figure 10 shows the LEMEs in the primary streamer tip and channel obtained from Eq. (3), satisfying all the conditions of Subsection 3.1 except for pressure. The effect of pressure on the LEME profile in the region of 4.6 mm to 5 mm away from the cathode is ignored. In the area of 1.8 mm to 4.6 mm away from the cathode, the LEME in the primary streamer tip increases as the pressure decreases. The electron-mean-free-path increases as the pressure decreases, and the electrons obtain more energy from the applied electric field. Therefore, the LEME in the primary streamer tip increases. The LEME in the primary streamer tip at 1 atm is approximately equal to that at 0.75 atm and is smaller than that at 0.5 atm in the region of 0 mm to 1.8 mm away from the cathode. The LEME in the primary streamer tip in the regions from 0 mm to 1.8 mm and from 4.6 mm to 5 mm away from the cathode is the result of the combined effect of the electrode and the gas pressure.

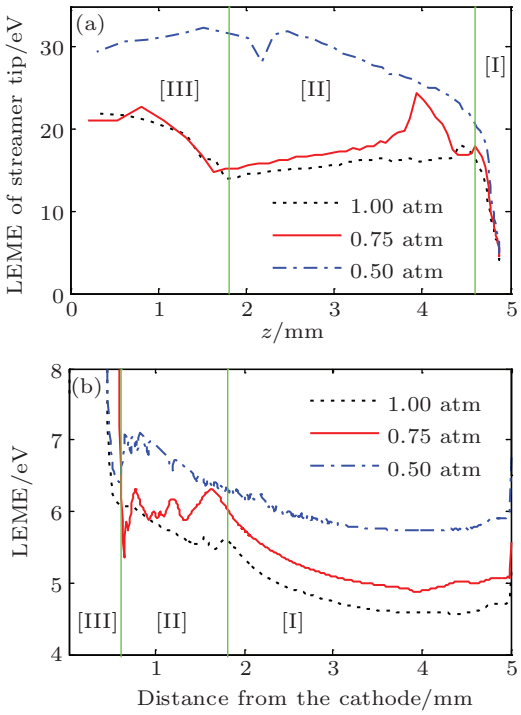


Fig. 10. (color online) LEME profiles in the primary streamer head with an oxygen and nitrogen mole ratio of 2:8: (a) LEME in the primary streamer head; (b) LEME in the primary streamer channel.

The LEME in the primary streamer tip reaches 30 eV at 0.5 atm, which is considerably larger than that at 1 atm and 0.75 atm. The 30 eV LEME is also slightly large for a primary streamer discharge. A large value is obtained because the kinetic scheme of the primary streamer reported in this study does not include the excitation process of gas molecules.

When the primary streamers bridge the gap, the LEME value in the primary streamer channel ranges from 4.5 eV to 7 eV. In the region of 1.8 mm to 5 mm away from the cathode, the difference between the LEMEs at 1 atm and 0.75 atm is approximately a constant of 1.17 eV. However, the difference between the LEMEs at 0.5 atm and 0.75 atm decreases from 2.08 eV to 0.66 eV when the distance from the cathode decreases. The LEME appears to fluctuate in the region of 0.6 mm to 1.8 mm away from the cathode.

The electric field and the reduced electric field distributions in the primary streamer tip are shown in Fig. 11. Based

on Figs. 10(a) and 11(a), the LEME in the primary streamer tip does not depend greatly on the electric field. However, the variation tendency of the LEME in the primary streamer tip is consistent with that of the reduced electric field as the pressure decreases, as shown in Figs. 10(a) and 11(b). The reduced electric field reflects the potential difference of the electron-mean-free-path and also determines the energy that the electrons obtain from the applied electric field on the electron-mean-free-path with the multi-component mole ratio given.[49]

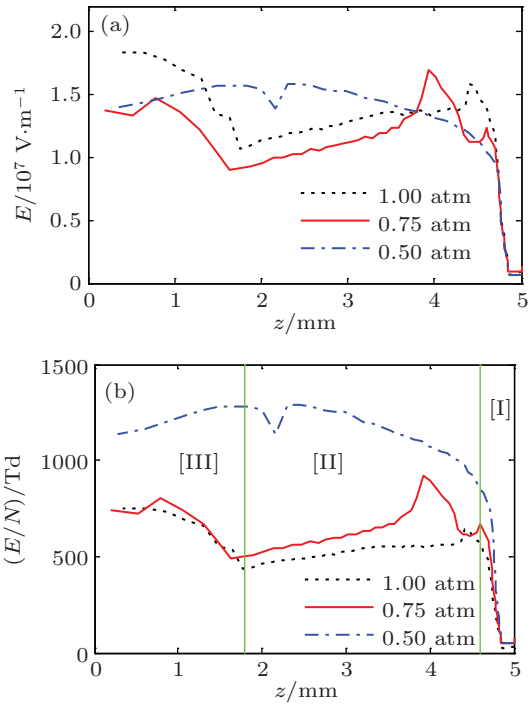


Fig. 11. (color online) (a) Electric field and (b) reduced electric field in the primary streamer tip with an oxygen and nitrogen mole ratio of 2:8.

4. Conclusions

The current study presented a detailed computational analysis of the pin-plate primary streamer discharge of a 5 mm pin-plate gap filled with oxygen–nitrogen mixture under an impulse voltage. The calculations gave detailed predictions of charge densities and electric fields as functions of time and position. The comparison of the electric field and streamer velocity obtained in the current study with the experimental and simulation results from the literature showed that the computational analysis of the primary streamer reported in the current study is valid. Furthermore, the effects of oxygen–nitrogen mole ratio and gas pressure on the LEME were investigated in oxygen–nitrogen mixtures with a pin-plate gap of 0.5 cm. The results are summarized as follows.

The LEME in the primary streamer tip increases as the oxygen–nitrogen mole ratio increases in the region of 0 mm to 4.6 mm away from the cathode. However, the LEME in the primary streamer channel increases as the oxygen–nitrogen mole ration decreases in the region of 2.3 mm to 5 mm away from the cathode. During the initial stage of the primary streamer, the effect of the oxygen–nitrogen mole ratio on the LEME in the primary streamer tip is ignored. In the primary streamer channel, the LEME ranges from 4.47 eV to 6 eV when the primary streamers bridge the gap.

The LEMEs in the primary streamer tip and channel increase as the pressure decreases in the region of 1.8 mm to 4.6 mm away from the cathode and in the region of 1.8 mm to 5 mm away from the cathode. The LEME in the primary streamer tip depends on the reduced electric field at fixed oxygen–nitrogen mole ratios.

The LEME increases to more than 30 eV as the gas pressure decreases or as the oxygen and nitrogen mole ratio increases. The aforementioned LEME value is slightly large for a primary streamer discharge. The slightly large value may have been obtained because the kinetic scheme does not include the excitation process of gas molecules. Future studies are recommended to determine how to simplify the kinetic scheme of a primary streamer under complex ambient conditions, such as electrical equipment insulation at high altitudes, i.e., at lower gas pressures.

References

[1] Wang X, Yang Q, Yao C, Zhang X and Sun C 2011 *Energies* **4** 2133
[2] Quoc An H, Pham Huu T, Le Van T, Cormier J M and Khacef A 2010 *Catalysis Today*
[3] Ono R and Oda T 2007 *J. Phys.* D: *Appl. Phys.* **40** 176
[4] Rossi F, Kylián O, Rauscher H, Hasiwa M and Gilliland D 2009 *New J. Phys.* **11** 115017
[5] Kutasi K, Guerra V and Sá P A 2011 *Plasma Sources Sci. Technol.* **20** 35006
[6] Takashima K, Adamovich I V, Xiong Z, Kushner M J, Starikovskaia S, Czarnetzki U and Luggenhölscher D 2011 *Phys. Plasmas* **18** 83505
[7] Kong M G, Shang W L and Wang D Z 2007 *Chin. Phys.* **16** 485
[8] Lü B, Wang X X, Luo H Y and Liang Z 2009 *Chin. Phys.* B **18** 646
[9] Zhao H Y and Mu Z X 2008 *Chin. Phys.* B **17** 1475
[10] Ebert U and Sentman D D 2008 *J. Phys.* D: *Appl. Phys.* **41** 230301
[11] Bourdon A, Pasko V P, Liu N Y, Célestin S, Ségur P and Marode E 2007 *Plasma Sources Sci. Technol.* **16** 656
[12] Ebert U, Brau F, Derks G, Hundsdorfer W, Kao C Y, Li C, Luque A, Meulenbroek B, Nijdam S and Ratushnaya V 2011 *Nonlinearity* **24** C1
[13] Ebert U, Montijn C, Briels T, Hundsdorfer W, Meulenbroek B, Rocco A and Van Veldhuizen E M 2006 *Plasma Sources Sci. Technol.* **15** S118
[14] Dujko S and Ebert U 2010 *7th ICRP and 63rd GEC*, October 4–8, 2010 Paris, France
[15] Chanrion O and Neubert T 2008 *J. Comput. Phys.* **227** 7222
[16] Li C, Ebert U and Brok W 2008 *IEEE Trans. Plasma Sci.* **36** 910
[17] Moss G D, Pasko V P, Liu N Veronis G 2006 *J. Geophys. Res.* **111** A2307
[18] Pancheshnyi S, Nudnova M and Starikovskii A 2005 *Phys. Rev.* E **71** 16407
[19] Georghiou G E, Papadakis A P, Morrow R and Metaxas A C 2005 *J. Phys.* D: *Appl. Phys.* **38** R303
[20] Hagelaar G J M and Pitchford L C 2005 *Plasma Sources Sci. Technol.* **14** 722
[21] Guo J M and Wu C H J 1993 *IEEE Trans. Plasma Sci.* **21** 684
[22] Li C, Brok W J M, Ebert U and Van der Mullen J 2007 *J. Appl. Phys.* **101** 123305
[23] Li C, Ebert U and Hundsdorfer W 2009 *J. Phys.* D: *Appl. Phys.* **42** 202003
[24] Li C, Ebert U and Hundsdorfer W 2010 *J. Comput. Phys.* **229** 200

[25] Li C, Ebert U and Hundsdorfer W 2012 *J. Comput. Phys.* **231** 1020
[26] Li C, Ebert U, Brok W J M and Hundsdorfer W 2008 *J. Phys.* D: *Appl. Phys.* 41 32004
[27] Kushner M J 2009 *J. Phys.* D: *Appl. Phys.* **42** 194013
[28] Farouk T, Farouk B, Staack D, Gutsol A and Fridman A 2006 *Plasma Sources Sci. Technol.* **15** 676
[29] Sima W X, Peng Q J, Yang Q, Yuan T and Shi J 2012 *IEEE Trans. Dielectr. Electr. Insul.* **19** 660
[30] Eichwald O, Ducasse O, Merbahi N, Yousfi M and Dubois D 2006 *J. Phys.* D: *Appl. Phys.* **39** 99
[31] Lifshitz E M and Pitaevskii L P 2008 *Physical Kinetics* (2nd edn) (Beijing: Peking Higher Education Press) pp. 98, 161–166 (in Chinese)
[32] Dujko S, Ebert U, White R D and Petrovic Z L 2011 *Jpn. J. Appl. Phys.* **50** 1J
[33] Pancheshnyi S V, Starikovskaia S M and Starikovskii A Y 2001 *J. Phys.* D: *Appl. Phys.* **34** 105
[34] Ségur P, Bourdon A and Marode E 2006 *Plasma Sources Sci. Technol.* **15** 648
[35] Guo S H 2008 *Electrodynamics* (3rd edn) (Beijing: Peking Higher Education Press) pp. 1–10 (in Chinese)
[36] Hagelaar G J M, De Hoog F J and Kroesen G M W 2000 *Phys. Rev.* E **62** 1452
[37] Boeuf J P and Pitchford L C 1995 *Phys Rev.* E **51** 1376
[38] Johnson A A and Tezduyar T E 1999 *Comput. Mech.* **23** 130
[39] Sentman D D, Stenbaek-Nielsen H C, McHarg M G and Morrill J S 2008 *J. Geophys. Res.* 113 D11112
[40] Gordillo-Vázquez F J 2008 *J. Phys.* D: *Appl. Phys.* **41** 234016
[41] Yuan X and Raja L L 2003 *IEEE Trans. Plasma Sci.* **31** 495
[42] Tanaka Y, Michishita T and Uesugi Y 2005 *Plasma Sources Sci. Technol.* **14** 134
[43] Kossyi I A, Kostinsky A Y, Matveyev A A and Silakov V P 1992 *Plasma Sources Sci. Technol.* **1** 207
[44] Yi W J and Williams P F 2002 *J. Phys.* D: *Appl. Phys.* **35** 205
[45] Luque A, Ratushnaya V and Ebert U 2008 *J. Phys.* D: *Appl. Phys.* **41** 234005
[46] Briels T M P, Kos J, Winands G J J, Van Veldhuizen E M and Ebert U 2008 *J. Phys.* D: *Appl. Phys.* **41** 234004
[47] Sigmond R S 1984 *J. Appl. Phys.* **56** 1355
[48] Winands G J J, Liu Z, Pemen A J M, Van Heesch E J M and Yan K 2008 *J. Phys.* D: *Appl. Phys.* **41** 234001
[49] Raizer Y P and Braun C 1992 *Gas Discharge Physics* (Heidelberg: Springer) p. 31